Journal of Materials Chemistry

Cite this: J. Mater. Chem., 2012, 22, 22135

www.rsc.org/materials

PAPER

Fine control of titania deposition to prepare C@TiO_2 composites and TiO_2 hollow particles for photocatalysis and lithium-ion battery applications†

Jun Ming,[abc] Yingqiang Wu,[abd] Srinivasan Nagarajan,[c] Dong-Ju Lee,[c] Yang-Kook Sun*[c] and Fengyu Zhao*[ab]

Received 25th June 2012, Accepted 4th September 2012
DOI: 10.1039/c2jm34106a

In this study, an effective method of slow hydrolization of metal alkoxide (*e.g.*, $Ti(C_4H_9O)_4$) in an ethanol–water system was systematically investigated and used to finely control the deposition of titania on carbon colloids. A model of adsorption–hydrolization of precursors during the coating process was rationally built for the first time to interpret the usability of the method and facilitate its further extension. Using this strategy, titania in the form of supported nanocrystals or layers on carbon colloids (TiO_2/C, C@TiO_2) was successfully tailored. Meanwhile, finely dispersed hollow TiO_2 nanoparticles with shells consisting of different crystalline structures were also prepared by varying the calcination conditions after removing the carbon cores. More importantly, the effects of the crystalline and nano/macrostructures of the as-prepared TiO_2 samples in photocatalysis and lithium-ion battery applications were analyzed in detail. The preliminary results show that anatase–rutile TiO_2 hollow particles demonstrate a higher catalytic activity in the photo-degradation of rhodamine B than anatase TiO_2 hollow particles, powders, and P25. However, in the case of Li-ion battery applications, the anatase TiO_2 hollow particles exhibited better performance as anode materials with high capacities of around 190 mA h g^{-1}, 140 mA h g^{-1}, and 120 mA h g^{-1} at current densities of 60 mA g^{-1}, 120 mA g^{-1}, and 300 mA g^{-1}, respectively, accompanied by stable cyclability.

Introduction

The preparation of nanostructured metal (oxides) and their composite materials is in high demand due to their intriguing performances in applications including catalysis,[1–3] sensors,[4–6] photovoltaics,[7–9] electrochemistry,[10–12] and biotechnology.[13–15] To synthesize specific materials, the choice of suitable precursors and a proper method is always important because it directly determines the properties of the resultant products.[3] To date, the most commonly used precursors include nitrates,[16–18] chlorides,[5,19,20] sulphates[21] and metal alkoxides.[22–25] The precursors are generally converted into metal (oxide) or intermediates *via* calcination,[20,26] precipitation,[5,27] deposition,[24,25,28] hydrolization,[23] or hydrothermal treatment,[21,29] largely depending on the precursors. However, among these precursors, the metal alkoxide group is highly reactive in hydrolization and/or precipitation, particularly for metallic ions (*e.g.*, Ti^{4+}, Si^{4+}, Zr^{4+}) that possess a high ionic charge to radius ratio.[23–25] The easier it is for a precursor to react, the more difficult it is to control the deposition process. This especially occurs in the well-known hard-template method, which needs precise tailoring of the metal (oxide) coating on templates for preparing composites and/or an inverse-structured metal (oxide).[30–33] Therefore, the development of an effective method to control the precipitation of easily hydrolizable precursors is significant to facilitate the preparation of the metal (oxide).

TiO_2 and TiO_2-based composite materials with anatase,[34] rutile,[35] hollandite,[36] ramsdellite[37] crystalline structures, and even an amorphous phase[38] have been widely prepared and applied in the fields of catalysis,[39,40] sensors,[41] dye-sensitized solar cells,[42] and lithium-ion batteries.[43,44] The reported excellent performances of TiO_2 strongly demonstrate that it is a promising material in these areas. However, the sensitive properties of TiO_2 depending on its structure and crystallinity,[45] together with the easy hydrolization of precursors (*e.g.*, $Ti(OC_3H_7)_4$,[46–48] $TiCl_4$,[49–51] TiF_4 (ref. 29 and 52)) even in an ambient atmosphere make it critical to control the hydrolization. Recently, a series of excellent works have been conducted to synthesize nanostructured

[a]*State Key Laboratory of Electroanalytical Chemistry, Changchun Institute of Applied Chemistry, Chinese Academy of Sciences, Changchun 130022, P. R. China. Fax: +86-0431-85262410; Tel: +86-0431-85262410*
[b]*Laboratory of Green Chemistry and Process, Changchun Institute of Applied Chemistry, Chinese Academy of Sciences, Changchun 130022, P. R. China. E-mail: zhaofy@ciac.jl.cn*
[c]*Department of WCU Energy Engineering, Hanyang University, 133-791, Republic of Korea. E-mail: yksun@hanyang.ac.kr; Fax: +82 2 2282 7329; Tel: +82 2 2220 0524*
[d]*Graduate University of the Chinese Academy of Sciences, Beijing 100049, P. R. China*

† Electronic supplementary information (ESI) available: Charaterization and detailed calculations of the adsorption/hydrolization model. Cycle performance of TiO_2 samples in the photodegradation of RhB. Comparative catalytic activities of TiO_2 samples in the photodegradation of benzene. The UV/visible diffuse reflectance absorption spectra of the TiO_2 samples. See DOI: 10.1039/c2jm34106a

TiO_2 based on the hard-template method,[29,52,53] but the process of precipitation/hydrolization and, in particular, the detailed coating behaviour of precursors on templates need to be further studied for TiO_2 and TiO_2-based derivatives such as the promising $Li_4Ti_5O_{12}$.[54,55]

In this work, we used the precursor of metal alkoxide (*e.g.*, $Ti(C_4H_9O)_4$) as an example and systematically investigated a method of slow hydrolization of the precursor in an ethanol–water system to finely control the deposition of titania on carbon colloids. A model of adsorption–hydrolization of precursors was built to simulate the coating process. Meanwhile, the results were evaluated to investigate the feasibility of facilitating its further extension to any other kind of easily hydrolyzable reaction. Based on this strategy, the titania in the form of supported nanocrystals or layers on carbon colloids (TiO_2/C, C@TiO_2) was successfully tailored at the nanoscale. Inspired by the widespread application of hollow structured particles,[56,57] hollow TiO_2 nanoparticles with a shell consisting of different crystalline structures were also prepared by varying the calcination conditions after removal of the carbon cores. More importantly, the effects of the crystalline and nano/micro-structures of the as-prepared TiO_2 samples were evaluated in photocatalysis and lithium-ion battery applications were analyzed in detail. The results are significant to guide and optimize the experimental conditions to effectively obtain materials with desired properties.

Experimental

Synthesis of C@$Ti(OH)_4$ and C@TiO_2

Carbon colloids were firstly synthesized *via* hydrothermal treatment of an aqueous glucose solution.[58,59] 0.1 g of the carbon colloids were well dispersed in 40 mL of ethanol under ultrasonication for 2 h in a glass bottle. Then, an appropriate amount of $Ti(C_4H_9O)_4$ was added into the colloidal solution under stirring. After 1 h of stirring in a sealed bottle, 70 mL of H_2O was added dropwise at a rate of 1 mL min^{-1}. Stirring was continued for another 12 h to allow complete hydrolyzation of the precursors. Finally, centrifugation was performed and brown solid powders of C@$Ti(OH)_4$ were obtained after drying the sample at 60 °C in an oven. Alternatively, C@TiO_2 composites were obtained followed by hydrothermal treatment of the primary solution of C@$Ti(OH)_4$ directly at 180 °C for 6 h. For comparison, blank $Ti(OH)_4$ powders were also prepared by the hydrolization of precursors in a solution without the presence of carbon colloids.

Preparation of hollow TiO_2

The brown solid powders of C@$Ti(OH)_4$ or C@TiO_2 were calcined applying specific procedures reported recently.[18] Firstly, calcination in a tube furnace under N_2 flow at 450 °C for 1 h (heating rate, 3 °C min^{-1}) and then recalcination under air flow while keeping the same thermal conditions were performed. As a result, hollow anatase TiO_2 particles (named hTiO_2) were obtained. Furthermore, hollow TiO_2 particles with different crystalline structures were prepared *via* further thermal treatment of the hTiO_2 at 600 °C or 700 °C for 3 h at a heating rate of 5 °C min^{-1}. The samples are designated as hTiO_2-600 and hTiO_2-700, respectively, based on the temperatures at which the samples were thermally treated. In addition, calcination of the $Ti(OH)_4$ powders under a similar procedure gave rise to TiO_2 powders, TiO_2-600, and TiO_2-700, which were used to compare their photocatalytic and electrochemical properties with the hollow powders.

Photocatalytic activity measurements

The photocatalytic activities of the TiO_2 samples were measured by the degradation of rhodamine B (RhB) in an aqueous solution. In a typical procedure, 100 mg of TiO_2 was dispersed firstly into 100 mL of RhB (10 ppm) and then the suspension was irradiated using a UV lamp (Spectroline SB-100P/F, 100 W, 8 cm away from the suspension) under stirring at room temperature. An electric fan was used to avoid heating of the suspension during irradiation. Before irradiation, the aqueous solution was magnetically stirred in the dark for 12 h to allow equilibrium adsorption of the dye on the catalytic surface. After initiation of the reaction by irradiation, 5 mL samples of the suspension were removed at regular intervals (5 min or 10 min) and centrifuged to completely remove the catalyst. The UV-visible absorption spectra of the centrifuged solution were recorded by a spectrophotometer.

Electrochemical measurements

The electrochemical experiments were carried out using a CR2025 coin-type cell. The cell composed of a working electrode and a lithium foil as the counter electrode, which were separated by a Celgard 2400 membrane. The working electrode consisted of an active material (as-prepared TiO_2 sample), acetylene black, and polymer binder (polyvinylidene difluoride, PVDF) at a weight ratio of 80 : 10 : 10. The electrolyte was 1 M $LiPF_6$ in a mixed solution of ethylene carbonate (EC)–dimethyl carbonate (DMC) (1 : 1 w/w). The cells were assembled in a dry argon-filled glove box with moisture and oxygen concentrations below 1 ppm. Galvanostatic charge–discharge cycles of the cells were performed in the voltage range between 3.0 V and 1.0 V at different current densities.

Results and discussion

Analysis of the coating process

Firstly, the hydrolization procedure was controlled by gradually adding water into the ethanol solution containing the precursors. The viewable hydrolization rate was also studied to obtain more details of the process (picture in the inset of Fig. 1a). The reason for dispersing precursors in ethanol is to dilute their concentration, thereby allowing controllable hydrolization and also enabling them to adsorb on a substrate (*e.g.*, carbon colloids) more easily and uniformly. Under slow addition of H_2O (1 mL min^{-1}), the precursor hydrolyzes to form $Ti(OH)_4$ based on the following reaction, $Ti(C_4H_9O)_4 + H_2O \rightarrow Ti(OH)_4 + C_4H_9OH$. The start time of the hydrolization, which was determined by the appearance of white precipitates, was evaluated as a function of the concentration of the precursors. As shown in Fig. 1a, the precipitation started about after 1 min at a concentration of 13.41 mmol L^{-1}, demonstrating that the rate of hydrolization could be finely controlled even for a high loading of TiO_2

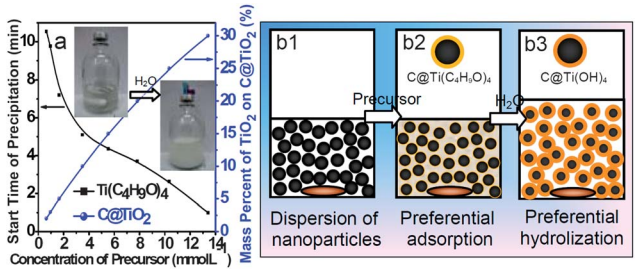

Fig. 1 (a) Start time of precipitation and the mass percent of TiO_2 on $C@TiO_2$ particles as functions of the concentration of the precursors in ethanol. The picture in the inset shows the equipment used for the reaction. (b1–b3) Schematic drawing of the coating process.

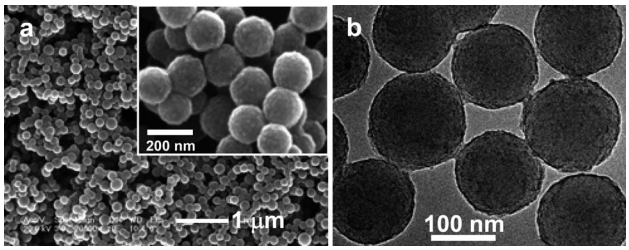

Fig. 2 (a and b) SEM and TEM images of $C@Ti(OH)_4$ particles.

(30 wt%) on $C@TiO_2$ particles. As the concentration was decreased to 0.64 mmol L^{-1}, corresponding to a low loading of TiO_2 (2 wt%), precipitation also occurred and its initial reaction time was delayed to 10.34 min. This strongly confirms that the approach of hydrolyzing the precursor in an ethanol–water system is feasible, even for very low concentrations.

During the coating process, we dispersed the carbon colloids well in ethanol to form a homogeneous colloidal solution and then added a certain amount of precursors to make them adsorb more easily on the as-dispersed carbon colloids for the following hydrolization, as shown in Fig. 1b1–b3. To prove that the precursor was enriched around the surface of the carbon colloids and to demonstrate the feasibility of this method, an adsorption–hydrolization model of the precursors was built (Fig. S1†). Firstly, the concentrations of the precursor before (C_0) and after ($C_{\text{after-adsorption}}$) adsorption in the solution were analyzed by inductively coupled plasma-atomic emission spectrometry (ICP-AES) to determine the molar amounts of precursor near the carbon particles ($n_{Ti(C_4H_9O)_4}$, Table 1). Meanwhile, the average radius of the carbon particles was R_0 (~77 nm)[18] and we assumed that the thickness of the precursor layer around the particles changed within 1–20 nm (yellow layer of $C@Ti(C_4H_9O)_4$, x = 1–20 nm, Fig. 1b2). Using the assumptions stated above, the volume of each carbon particle (V_0) and $C@Ti(C_4H_9O)_4$ particle ($V_{0-x\text{nm}}$) could be calculated as $4\pi R_0^3/3$ and $4\pi R_x^3/3$, respectively (R_x: the radius of $C@Ti(C_4H_9O)_4$, $R_x = R_0 + x$). As a result, the individual space volume around each carbon particle ($V_{0\text{space-}x\text{nm}}$, x = 1–20 nm) could be calculated as the difference of V_0 and $V_{0-x\text{nm}}$, which is $4\pi(R_x^3 - R_0^3)/3$. Subsequently, the total volume of space around the particles ($V_{\text{total space-}x\text{nm}}$) could be derived as the product of the number of carbon colloids ($N_{\text{carbon-colloids}}$) and the individual space volume around each carbon particle ($V_{0\text{space-}x\text{nm}}$) ($V_{\text{total space-}x\text{nm}} = N_{\text{carbon-colloids}} \times V_{0\text{space-}x\text{nm}}$). Finally, the concentration of the precursor enriched in these spaces could be obtained ($C_{x\text{nm}} = n_{Ti(C_4H_9O)_4}/V_{\text{total space-}x\text{nm}}$) and these values were designated as $C_{1\text{nm}}$, $C_{5\text{nm}}$, $C_{10\text{nm}}$ and $C_{15\text{nm}}$, according to the supposed thickness of the precursor layer, as shown in Table 1 and the detailed calculations provided in the ESI.†

As shown in Table 1, the concentration of precursors within the 1–20 nm layer ($C_{x\text{nm}}$) around the carbon particles was always much higher than that in the bulk solution ($C_{\text{after-adsorption}}$), demonstrating the richness of the precursor around the particles and also confirming the effectiveness of applying preferential hydrolization. Taking the 20 wt% TiO_2 loading as an example, the concentrations of the precursors in the solution before and after adsorption were 7.82 mmol L^{-1} and 6.53 mmol L^{-1}, respectively, whereas the concentrations around the particles within 10–20 nm were as high as 2821 and 1250 mmol L^{-1}, respectively (Table 1). Hence, the hydrolization process becomes an obvious phenomenon on carbon colloids immediately after the introduction of water, rather than in solution. This is evident because the lower concentration (6.53 mmol L^{-1}) requires at least 4.05 min for precipitation to begin (Fig. 1a), without consideration of the diffusion of precursors from the bulk solution to the surface of particles accompanying the decrease of the concentration around the particles during the hydrolization. As a result, the deposition process could be finely controlled and the formation of free $Ti(OH)_4$ could be successfully avoided. The scanning electron micrograph (SEM) and transmission electron micrograph (TEM) of the $C@Ti(OH)_4$ particles directly confirm the feasibility of the method and the rationale of the analysis because a uniform layer of $Ti(OH)_4$ was coated on the carbon colloids without any formation of free $Ti(OH)_4$, even at a high loading of 30.0 wt% (Fig. 2a and b). Good knowledge of the adsorption–hydrolization process could be helpful to design and control the amount of precursor used, particularly for easily hydrolyzable precursors. Moreover, a series of multifunctional core–shell and

Table 1 Concentrations of the precursors in the solution and around carbon colloids[a]

m_{TiO_2}%	C_0 mmol L^{-1}	$C_{\text{after-adsorption}}$ mmol L^{-1}	$C_{1\text{nm}}$ mmol L^{-1}	$C_{5\text{nm}}$ mmol L^{-1}	$C_{10\text{nm}}$ mmol L^{-1}	$C_{20\text{nm}}$ mmol L^{-1}
30	13.41	11.82	—	—	—	1563
20	7.82	6.53	—	—	2821	1250
10	3.48	3.11	—	1735	814	361
2	0.64	0.39	—	1173	551	244

[a] m_{TiO_2}: mass percent loading of TiO_2 on $C@TiO_2$ particles; $n_{Ti(C_4H_9O)_4} = (C_0 - C_{\text{after-adsorption}}) \times 40$ mL, 40 mL is the volume of solution; $C_{x\text{nm}}$: concentration of precursors around the carbon colloids within the range of x nm.

hollow-structured TiO_2 materials could be further prepared based on the obtained $C@Ti(OH)_4$.

Formation of $C@TiO_2$ particles

In the past few decades, hollow oxide particles have been prepared using carbon particles as a template because the carbon inevitably burned off during the process of crystallization of the oxide under calcination.[5,18,20] Only a few studies have focused on trying to preserve the carbon cores.[59] Alternatively, it is promising to preserve the carbon cores in some cases because the conductive, inert, and durable properties of carbon cores could not only enhance the structural stability, but also reinforce the conductive ability of the metal oxide in addition to the unique core–shell structure, leading to great potential applications in various areas. Herein, the core–shell structured TiO_2/C and $C@TiO_2$ particles with supported nanocrystals or a layer of TiO_2 nanocrystals were prepared *via* further hydrothermal treatment of the solution after hydrolization.

Compared with the smooth surface of the $C@Ti(OH)_4$ particles, a rough layer of TiO_2 nanocrystals that originated from the crystallization of amorphous $Ti(OH)_4$ was present on the carbon colloids, as shown in the SEM and TEM images (Fig. 3a and b). The X-ray powder diffraction (XRD) pattern confirms that the anatase crystalline structure was obtained (JCPDS-#83-2243) (Fig. 4a and b). The wide and medium (101) peak reflects the random accumulation of TiO_2 nanocrystals, which agrees well with the polycrystalline layer on the carbon cores, as observed in the TEM and high resolution TEM (HRTEM) photographs (Fig. 3b and c). Even with a thick and rough layer of TiO_2 (30 wt%) nanocrystals present, these composite particles still have a uniform coating and preserve good dispersion. It is noteworthy that the thickness of the shell was within the range of 5.58–13.47 nm and the average value was around 9.35 nm, which supports the rationality of the suppositional precursor layer (~20 nm) in the adsorption–hydrolization model. Furthermore, the loading

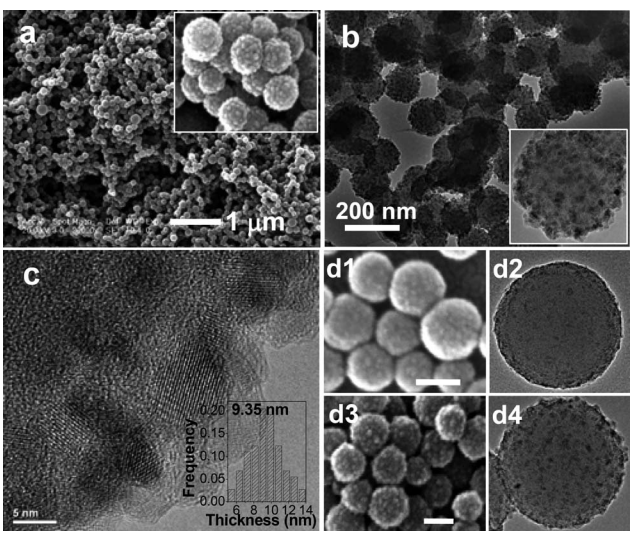

Fig. 3 (a–c) SEM, TEM, and HRTEM images of $C@TiO_2$ particles with a TiO_2 loading of 30%. (d1–d4) SEM and TEM images of TiO_2/C and $C@TiO_2$ particles with 5 wt% and 20 wt% TiO_2. The unlabelled scale bar is 100 nm.

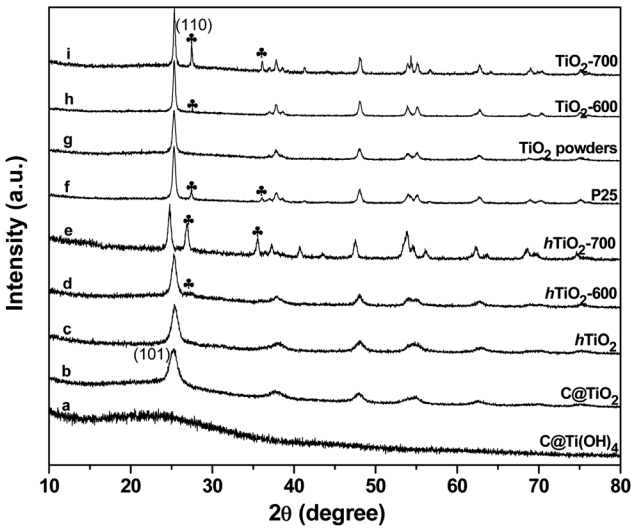

Fig. 4 XRD patterns of as-prepared TiO_2 samples prepared under different conditions.

amount of TiO_2 nanocrystals could be precisely tuned by varying the concentration of the precursors, thereby giving rise to supported TiO_2/C and core–shell structured $C@TiO_2$ particles to meet diverse requirements in applications (Fig. 3d1–d4). Obviously, this method provides an effective way to fabricate TiO_2–carbon or other TiO_2-based composite materials with a polycrystalline surface. Moreover, in addition to TiO_2, any other oxide-based composite materials could be prepared using this strategy, particularly when it is required to preserve the carbon substrate while still facilitating crystallization of the oxide.

Preparation of hollow TiO_2

To date, numerous hollow-structured TiO_2 with different morphologies have been prepared and have performed well in photocatalysis and lithium-ion battery applications.[29,52,60,61] However, limited attention has been paid to investigating various crystalline hollow TiO_2 nanoparticles, which may possess quite different properties. Herein, hollow TiO_2 nanoparticles with different crystalline structures were synthesized by varying the calcination conditions after removing the carbon cores. The SEM and TEM images show that the as-prepared hollow TiO_2 nanoparticles maintained good dispersion and a spherical structure after calcination of $C@Ti(OH)_4$ by following a specific procedure under N_2/air at a temperature of 450 °C,[18] where some of them are open-structured semi-spherical particles (Fig. 5a–c) and contain traces of carbon (1.3 wt%) as determined by the CHN-analysis. The XRD results show that the hollow TiO_2 has a crystalline anatase structure (JCPDS-#83-2243) (Fig. 4c). Its characteristic peaks are similar to that of $C@TiO_2$ (Fig. 4b), further demonstrating that hydrothermal crystallization of TiO_2 is as effective as calcination and the shell of hollow nanoparticles also consisted of numerous TiO_2 nanocrystals (Fig. S2a†). Further thermal treatment of hollow anatase TiO_2 for 3 h at temperatures of 600 °C and 700 °C gave rise to mixed anatase and rutile phase hollow TiO_2 nanoparticles ($hTiO_2$-600, $hTiO_2$-700). These particles have different crystalline structures depending on the processing temperature. $hTiO_2$-600 contained

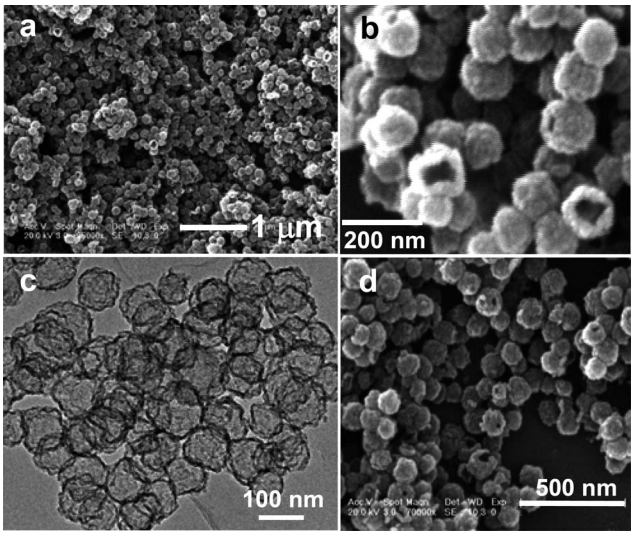

Fig. 5 (a–c) SEM and TEM images of hollow TiO_2 nanoparticles. (d) SEM photograph of aggregated hollow TiO_2 nanoparticles.

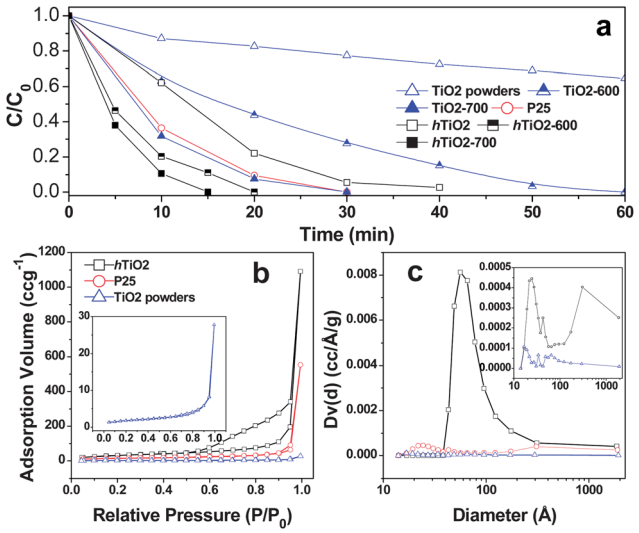

Fig. 6 (a) Catalytic performance of the TiO_2 samples assessed by the photo-degradation of RhB. (b) Nitrogen adsorption–desorption isotherms and (c) pore size distribution of the TiO_2 samples. The inset in (b) shows an enlargement of TiO_2 powders and the inset in (c) shows an enlargement of TiO_2 powders and P25.

only a trace amount of rutile (PDF-#73-1764), while $hTiO_2$-700 contained both anatase and rutile (Fig. 4d and e). An obvious peak shift existed in the XRD patterns of $hTiO_2$-700 relative to anatase and rutile, which probably resulted from the complete combination of these two phases. Fortunately, the samples could still maintain good dispersion and a spherical morphology even after thermal treatment at high temperature (Fig. 4d), fully demonstrating the physical stability of the hollow structure. Alternatively, calcination of $C@TiO_2$ could also give rise to hollow TiO_2 nanoparticles but aggregation and collapse seem to occur easily (Fig. S2b†). The reason for this behaviour can probably be ascribed to the rough layers of TiO_2 nanocrystals on $C@TiO_2$, which pose a negative effect on the formation of the intact shell during the process of removal of the carbon cores.

Photocatalysis and lithium-ion battery applications

Many publications have reported that hollow TiO_2 particles have higher photo-catalytic properties due to the high specific surface area and rich pores.[60–62] In our experiments, we determined that the photocatalytic activity of anatase $hTiO_2$ nanoparticles for the photo-degradation of RhB is lower than that of the commercial P25 (Fig. 6a). It seems that the crystallinity of TiO_2 plays a predominant role in determining the catalytic properties, even though the BET surface area and pore volume of $hTiO_2$ (117 m^2 g^{-1}, 1.789 cm^3 g^{-1}) were about double those of P25 (50.85 m^2 g^{-1}, 0.8578 cm^3 g^{-1}) (Fig. 6b and c). With the presence of a rutile phase (110) in the shell of the hollow nanoparticles, the catalytic abilities of $hTiO_2$-600 and $hTiO_2$-700 increased drastically and were higher than those of P25, as shown in Fig. 5a. Similarly, the TiO_2 powders (JCPDS#-73-1764) that were directly hydrolyzed from precursors also exhibited a similar trend in the catalytic performance as TiO_2-600 (JCPDS-#84-1285 (anatase) trace of rutile) and TiO_2-700 (JCPDS-#89-4921 (anatase) and JCPDS-#84-1283 (rutile)). The catalytic ability increased as the presence of rutile increased in the sample (Fig. 4g–i). These results confirm that the presence of rutile in the anatase phase positively enhances the catalytic properties. This phenomenon was further confirmed by the photo-degradation of contaminants such as benzene organic compounds which show a similar trend in their photocatalytic properties depending on their crystallinity (Fig. S3†). It is noteworthy that the traces of carbon that existed in anatase $hTiO_2$ show limited effects on the catalytic performance compared to the crystallinity effects (Fig. S4†). Due to the secondary factor of nano/microstructures such as the high surface area and rich pores, the hollow TiO_2 particles always demonstrated a higher catalytic performance than the TiO_2 powders (6.328 m^2 g^{-1}, 0.043 cm^3 g^{-1}) with a similar crystalline structure, accompanying an excellent cycle performance (Fig. S4†). It is noteworthy that even with a low surface area and poor pores, the catalytic ability of the TiO_2 powders was largely enhanced close to that of P25 after calcination at 700 °C for 3 h (TiO_2-700). This further proves that controlling the kind and degree of crystallinity seems to be more critical in tuning the catalytic activity and even selectivity of TiO_2 in some cases.[61,63]

In contrast, the presence of a rutile phase in the TiO_2 structure seems to have a negative effect on the electrochemical performance in lithium-ion batteries when used as an anode material. For example, the capacity of P25 decayed drastically from 180 mA h g^{-1} to 39 mA h g^{-1} (21.67% capacity retention) after 100 cycles at a current density of 60 mA g^{-1}. A similar decay also occurred with the $hTiO_2$-600 sample (182 mA h g^{-1} to 98 mA h g^{-1}, 53.85% capacity retention) compared to the primary anatase $hTiO_2$. The $hTiO_2$ nanoparticles displayed an initial charging capacity of 203 mA h g^{-1} and a reversible capacity of 187 mA h g^{-1} at a current density of 60 mA h g^{-1}, with a 92% capacity retention at the end of 100 cycles (Fig. 7a). Increasing the current density to 150 mA g^{-1} and 300 mA g^{-1} for 100 cycles resulted in good cyclability together with high capacities of around 140 and 120 mA h g^{-1}, respectively, which were well preserved (Fig. 7a). Meanwhile, the anatase TiO_2 powders, even though they have a

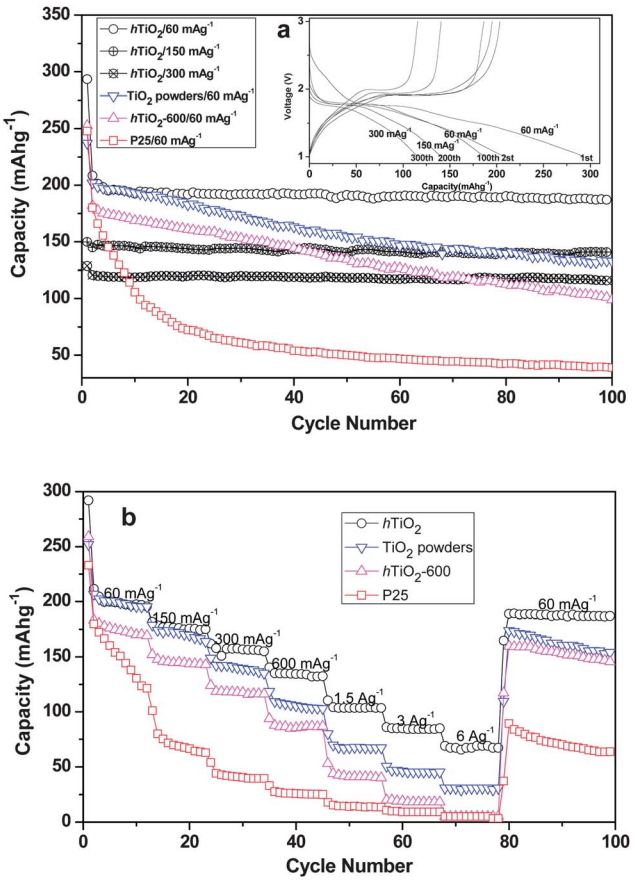

Fig. 7 Comparative cycling performance of as-prepared TiO_2 samples (a) for 100 cycles and (b) at different current densities. The inset in (a) shows the typical charge–discharge voltage profiles of $hTiO_2$ nanoparticles.

low surface area, still show a better performance (201 mA h g^{-1} *vs.* 131 mA h g^{-1}, 65% capacity retention) than $hTiO_2$-600, demonstrating that the rutile phase in the structure of TiO_2 largely affects the electrochemical properties. The reason should be ascribed to the diffusion coefficient of lithium ions in rutile TiO_2 (1.42×10^{-13} cm^2 s^{-1}), which is smaller than that of anatase TiO_2 (1.81×10^{-13} cm^2 s^{-1}),[64] which is probably due to the fact that the channels of rutile TiO_2 are narrower than those of anatase TiO_2. However, the performances of the anatase TiO_2 powders were not as good as those of the anatase $hTiO_2$ particles, particularly at a high current density (Fig. 7b). This behaviour can be ascribed to two reasons: (i) the higher crystalline degree (Fig. 4g) and (ii) the low surface area of the TiO_2 powders. As previously reported,[34,64] an increase in the crystallinity retards the diffusion of lithium in anatase TiO_2, while $hTiO_2$ nanoparticles with a thin wall consisting of numerous polycrystalline nanocrystals could largely facilitate the insertion/extraction of lithium ions. The negative effects due to the presence of rutile TiO_2 and high crystallinity were more obvious at high current densities of 1.5, 3, and 6 A g^{-1}, leading to the drastic decrease of the capacities of the P25, $hTiO_2$-600, and TiO_2 powders (Fig. 7b). Promisingly, the capacity of the anatase $hTiO_2$ nanoparticles could be well preserved at high current densities and was still around 70 mA h g^{-1} at a current density of 6 A g^{-1} (~36 C, where 1 C = 167 mA h g^{-1}). After the high-rate cycle, the capacity of the anatase $hTiO_2$ nanoparticles could return to the primary value at a current density of 60 mA h g^{-1}, demonstrating the good cyclability of the materials. In brief, three aspects are responsible for the high capacity and good cyclability of the anatase $hTiO_2$ nanoparticles: (i) suitable degree of crystallinity, (ii) anatase structure, and (iii) hollow spherical structure with a high surface area and thin wall consisting of numerous nanocrystals. Based on the above analysis, further investigations are ongoing to optimize the crystallization of as-prepared TiO_2 powders to check whether the good properties such as their promising capacity and cycle behaviour in the first 20 cycles could be maintained even with a low surface area (Fig. 7).

Conclusions

In this study, the approach of slow hydrolization of metal alkoxide (*e.g.*, $Ti(C_4H_9O)_4$) in a water–ethanol system was investigated and successfully used to control the deposition of titania on carbon colloids. An adsorption and hydrolization model was built for the first time to show the feasibility of this method. Meanwhile, the coating process and behaviour were discussed in detail to facilitate its further extension for other easily hydrolizable precursors. Based on this strategy, not only were the support and layers of TiO_2 nanocrystals (TiO_2/C, C@TiO_2) on carbon colloids precisely tailored, finely dispersed hollow TiO_2 nanoparticles consisting of different kinds and degrees of crystalline structures were prepared. The effects of crystallinity and nano/macrostructures of the as-prepared TiO_2 samples on their performances in photocatalysis and lithium-ion battery applications were also evaluated in detail. The results show that the presence of rutile in the TiO_2 structure positively enhances the photocatalytic properties but seems to negatively affect the insertion/extraction of lithium ions when used as an anode material. Meanwhile, a large sample surface area is beneficial to enhance the catalytic and electrochemical properties but is not the main factor in some cases. For these reasons, as-prepared anatase–rutile TiO_2 hollow particles demonstrated the highest catalytic activity in the photo-degradation of RhB among the anatase $hTiO_2$, TiO_2 powders, and P25 samples, while the anatase hollow TiO_2 particles demonstrated a high capacity and good cyclability in the lithium-ion battery application. With further knowledge of the coating behaviour and the effects of the kind and degree of crystallinity and nano/microstructures on the properties, it could be easier to design and optimize the experimental conditions to produce desired materials.

Acknowledgements

This work was financially supported by the One Hundred Talent Program of CAS, NSFC 20873139, and KJCX2, YWH16. This research was also supported by the Human Resources Development program (No. 20114010203150) of the Korea Institute of Energy Technology Evaluation and Planning (KETEP) grant funded by the Korea government Ministry of Knowledge Economy and the National Research Foundation of Korea (NRF) grant funded by the Korea government (MEST) (no. 2009-0092780).

Notes and references

1 Y. D. Yin, R. M. Rioux, C. K. Erdonmez, S. Hughes, G. A. Somorjai and A. P. Alivisatos, *Science*, 2004, **304**, 711–714.
2 M.-R. Gao, Y.-F. Xu, J. Jiang, Y.-R. Zheng and S.-H. Yu, *J. Am. Chem. Soc.*, 2012, **134**, 2930–2933.
3 J. R. A. Sietsma, J. D. Meeldijk, J. P. den Breejen, M. Versluijs-Helder, A. J. van Dillen, P. E. de Jongh and K. P. de Jong, *Angew. Chem., Int. Ed.*, 2007, **46**, 4547–4549.
4 X. Chen, Z. Guo, W.-H. Xu, H.-B. Yao, M.-Q. Li, J.-H. Liu, X.-J. Huang and S.-H. Yu, *Adv. Funct. Mater.*, 2011, **21**, 2049–2056.
5 X. M. Sun, J. F. Liu and Y. D. Li, *Chem.–Eur. J.*, 2006, **12**, 2039–2047.
6 J. Zhang, X. Liu, S. Wu, M. Xu, X. Guo and S. Wang, *J. Mater. Chem.*, 2010, **20**, 6453.
7 S. C. Yang, D. J. Yang, J. Kim, J. M. Hong, H. G. Kim, I. D. Kim and H. Lee, *Adv. Mater.*, 2008, **20**, 1059–1064.
8 I. Robel, M. Kuno and P. V. Kamat, *J. Am. Chem. Soc.*, 2007, **129**, 4136.
9 J. T. Park, R. Patel, H. Jeon, D. J. Kim, J. S. Shin and J. H. Kim, *J. Mater. Chem.*, 2012, **22**, 6131–6138.
10 H.-G. Jung, J. Kim, B. Scrosati and Y.-K. Sun, *J. Power Sources*, 2011, **196**, 7763–7766.
11 V. Chakrapani, K. Tvrdy and P. V. Kamat, *J. Am. Chem. Soc.*, 2010, **132**, 1228.
12 X. W. Lou, Y. Wang, C. L. Yuan, J. Y. Lee and L. A. Archer, *Adv. Mater.*, 2006, **18**, 2325.
13 P. Yang , Q.-Z. Xu, S.-Y. Jin, Y. Zhao, Y. Lu, X.-W. Xu and S.-H. Yu, *Chem.–Eur. J.*, 2012, **18**, 1154–1160.
14 W.-P. Xu, L.-C. Zhang, J.-P. Li, Y. Lu, H.-H. Li, Y.-N. Ma, W.-D. Wang and S.-H. Yu, *J. Mater. Chem.*, 2011, **21**, 4593.
15 Y. H. Deng, C. H. Deng, D. W. Qi, C. Liu, J. Liu, X. M. Zhang and D. Y. Zhao, *Adv. Mater.*, 2009, **21**, 1377–1382.
16 J. Roggenbuck and M. Tiemann, *J. Am. Chem. Soc.*, 2005, **127**, 1096–1097.
17 B. Z. Tian, X. Y. Liu, H. F. Yang, S. H. Xie, C. Z. Yu, B. Tu and D. Y. Zhao, *Adv. Mater.*, 2003, **15**, 1370.
18 J. Ming, Y. Wu, L. Wang, Y. Yu and F. Zhao, *J. Mater. Chem.*, 2011, **21**, 17776.
19 J. Ming, R. X. Liu, G. F. Liang, H. Y. Cheng, Y. C. Yu and F. Y. Zhao, *J. Mater. Chem.*, 2011, **21**, 10929–10934.
20 X. Sun and Y. Li, *Angew. Chem., Int. Ed.*, 2004, **43**, 3827–3831.
21 M. M. Titirici, M. Antonietti and A. Thomas, *Chem. Mater.*, 2006, **18**, 3808–3812.
22 X. C. Guo and P. Dong, *Langmuir*, 1999, **15**, 5535–5540.
23 P. M. Arnal, C. Weidenthaler and F. Schuth, *Chem. Mater.*, 2006, **18**, 2733–2739.
24 J. D. Holmes, *Science*, 2000, **287**, 1471–1473.
25 K. M. Ryan, D. Erts, H. Olin, M. A. Morris and J. D. Holmes, *J. Am. Chem. Soc.*, 2003, **125**, 6284–6288.
26 B. Z. Tian, X. Y. Liu, L. A. Solovyov, Z. Liu, H. F. Yang, Z. D. Zhang, S. H. Xie, F. Q. Zhang, B. Tu, C. Z. Yu, O. Terasaki and D. Y. Zhao, *J. Am. Chem. Soc.*, 2004, **126**, 865–875.
27 J. Y. Gong, S. R. Guo, H. S. Qian, W. H. Xu and S. H. Yu, *J. Mater. Chem.*, 2009, **19**, 1037–1042.
28 J. Ming, C. Wu, H. Cheng, Y. Yu and F. Zhao, *J. Supercrit. Fluids*, 2011, **57**, 137–142.
29 X. W. Lou and L. A. Archer, *Adv. Mater.*, 2008, **20**, 1853.
30 F. Caruso, R. A. Caruso and H. Mohwald, *Science*, 1998, **282**, 1111–1114.
31 J. C. Hulteen and C. R. Martin, *J. Mater. Chem.*, 1997, **7**, 1075–1087.
32 Y. Deng, D. Qi, C. Deng, X. Zhang and D. Zhao, *J. Am. Chem. Soc.*, 2008, **130**, 28.
33 A. H. Lu and F. Schüth, *Adv. Mater.*, 2006, **18**, 1793–1805.
34 M. Wagemaker, A. P. M. Kentgens and F. M. Mulder, *Nature*, 2002, **418**, 397–399.
35 K. N. P. Kumar, K. Keizer, A. J. Burggraaf, T. Okubo and H. Nagamoto, *J. Mater. Chem.*, 1993, **3**, 923–929.
36 L. D. Noailles, C. S. Johnson, J. T. Vaughey and M. M. Thackeray, *J. Power Sources*, 1999, **81**, 259–263.
37 A. Kuhn, R. Amandi and F. Garcia-Alvarado, *J. Power Sources*, 2001, **92**, 221–227.
38 M. Hibino, K. Abe, M. Mochizuki and M. Miyayama, *J. Power Sources*, 2004, **126**, 139–143.
39 X. Meng, H. Cheng, S.-i. Fujita, Y. Hao, Y. Shang, Y. Yu, S. Cai, F. Zhao and M. Arai, *J. Catal.*, 2010, **269**, 131–139.
40 J. S. Chen, D. Y. Luan, C. M. Li, F. Y. C. Boey, S. Z. Qiao and X. W. Lou, *Chem. Commun.*, 2010, **46**, 8252–8254.
41 A. M. Ruiz, G. Sakai, A. Cornet, K. Shimanoe, J. R. Morante and N. Yamazoe, *Sens. Actuators, B*, 2003, **93**, 509–518.
42 H. J. Tian, L. H. Hu, C. N. Zhang, S. H. Chen, J. A. Sheng, L. Mo, W. Q. Liu and S. Y. Dai, *J. Mater. Chem.*, 2011, **21**, 863–868.
43 J. S. Chen, J. Liu, S. Z. Qiao, R. Xu and X. W. Lou, *Chem. Commun.*, 2011, **47**, 10443.
44 H. G. Jung, C. S. Yoon, J. Prakash and Y. K. Sun, *J. Phys. Chem. C*, 2009, **113**, 21258–21263.
45 Y. Ren, Z. Liu, F. Pourpoint, A. R. Armstrong, C. P. Grey and P. G. Bruce, *Angew. Chem., Int. Ed.*, 2012, **51**, 2164–2167.
46 H. Ming, Z. Ma, H. Huang, S. Lian, H. Li, X. He, H. Yu, K. Pan, Y. Liu and Z. Kang, *Chem. Commun.*, 2011, **47**, 8025.
47 Y. G. Guo, Y. S. Hu, W. Sigle and J. Maier, *Adv. Mater.*, 2007, **19**, 2087.
48 L. Zhao, X. Chen, X. Wang, Y. Zhang, W. Wei, Y. Sun, M. Antonietti and M.-M. Titirici, *Adv. Mater.*, 2010, **22**, 3317–3321.
49 H.-G. Jung, S. W. Oh, J. Ce, N. Jayaprakash and Y.-K. Sun, *Electrochem. Commun.*, 2009, **11**, 756–759.
50 D. H. Kim, J. S. Jang, S. S. Han, K. S. Lee, S. H. Choi, A. Umar, J. W. Lee, D. W. Shin, S. T. Myung, J. S. Lee, S. J. Kim, Y. K. Sun and K. S. Lee, *J. Phys. Chem. C*, 2009, **113**, 14034–14039.
51 E. L. Crepaldi, G. J. D. A. Soler-Illia, D. Grosso, F. Cagnol, F. Ribot and C. Sanchez, *J. Am. Chem. Soc.*, 2003, **125**, 9770–9786.
52 Z. Wang and X. W. D. Lou, *Adv. Mater.*, 2012, **24**, 4124–4129.
53 S.-T. Myung, N. Takahashi, S. Komaba, C. S. Yoon, Y.-K. Sun, K. Amine and H. Yashiro, *Adv. Funct. Mater.*, 2011, **21**, 3231–3241.
54 H.-G. Jung, S.-T. Myung, C. S. Yoon, S.-B. Son, K. H. Oh, K. Amine, B. Scrosati and Y.-K. Sun, *Energy Environ. Sci.*, 2011, **4**, 1345.
55 H.-G. Jung, M. W. Jang, J. Hassoun, Y.-K. Sun and B. Scrosati, *Nat. Commun.*, 2011, **2**, 516.
56 X. W. Lou, L. A. Archer and Z. Yang, *Adv. Mater.*, 2008, **20**, 3987–4019.
57 Z. Wang, L. Zhou and X. W. David Lou, *Adv. Mater.*, 2012, **24**, 1903–1911.
58 X. M. Sun and Y. D. Li, *Angew. Chem., Int. Ed.*, 2004, **43**, 597–601.
59 J. Ming, H. Cheng, Y. Yu, Y. Wu and F. Zhao, *J. Mater. Chem.*, 2011, **21**, 6654.
60 Z. D. Yao, W. Wei, J. L. Wang, J. Yang and Y. N. Nuli, *Acta Phys.-Chim. Sin.*, 2011, **27**, 1005–1016.
61 S. W. Liu, J. G. Yu and M. Jaroniec, *J. Am. Chem. Soc.*, 2010, **132**, 11914–11916.
62 T. Zhang, L. Ge, X. Wang and Z. Gu, *Polymer*, 2008, **49**, 2898–2902.
63 Y. Aoyama, Y. Oaki, R. Ise and H. Imai, *CrystEngComm*, 2012, **14**, 1405–1411.
64 K. Kanamura, K. Yuasa and Z. Takehara, *J. Power Sources*, 1987, **20**, 127–134.